PNAS RESEARCH ARTICLE | IMMUNOLOGY AND INFLAMMATION

Tankyrases inhibit innate antiviral response by PARylating VISA/MAVS and priming it for RNF146-mediated ubiquitination and degradation

Yan-Ran Xu[a,b,c,1], Meng-Ling Shi[a,b,c,1], Yu Zhang[d,1], Na Kong[a,b,c], Cong Wang[a,b,c], Yi-Feng Xiao[a,b], Shi-Shen Du[b], Qi-Yun Zhu[e], and Cao-Qi Lei[a,b,c,2]

Edited by George Stark, Cleveland Clinic Lerner Research Institute, Cleveland, OH; received December 22, 2021; accepted April 25, 2022

During viral infection, sensing of viral RNA by retinoic acid–inducible gene-I–like receptors (RLRs) initiates an antiviral innate immune response, which is mediated by the mitochondrial adaptor protein VISA (virus-induced signal adaptor; also known as mitochondrial antiviral signaling protein [MAVS]). VISA is regulated by various post-translational modifications (PTMs), such as polyubiquitination, phosphorylation, *O*-linked *β*-d-*N*-acetylglucosaminylation (O-GlcNAcylation), and monomethylation. However, whether other forms of PTMs regulate VISA-mediated innate immune signaling remains elusive. Here, we report that Poly(ADP-ribosyl)ation (PARylation) is a PTM of VISA, which attenuates innate immune response to RNA viruses. Using a biochemical purification approach, we identified tankyrase 1 (TNKS1) as a VISA-associated protein. Viral infection led to the induction of TNKS1 and its homolog TNKS2, which translocated from cytosol to mitochondria and interacted with VISA. TNKS1 and TNKS2 catalyze the PARylation of VISA at Glu137 residue, thereby priming it for K48-linked polyubiquitination by the E3 ligase Ring figure protein 146 (RNF146) and subsequent degradation. Consistently, TNKS1, TNKS2, or RNF146 deficiency increased the RNA virus–triggered induction of downstream effector genes and impaired the replication of the virus. Moreover, TNKS1- or TNKS2-deficient mice produced higher levels of type I interferons (IFNs) and proinflammatory cytokines after virus infection and markedly reduced virus loads in the brains and lungs. Together, our findings uncover an essential role of PARylation of VISA in virus-triggered innate immune signaling, which represents a mechanism to avoid excessive harmful immune response.

RNA virus | VISA | TNKS | PARylation | innate immune response

Significance

Virus-induced signal adaptor (VISA)/mitochondrial antiviral signaling protein (MAVS) is an essential adaptor protein in innate immune response to RNA viruses; understanding how VISA is regulated is important for the treatment of infectious diseases. In this study, we discovered that tankyrase 1 (TNKS1) and TNKS2 negatively regulate innate antiviral response by catalyzing Poly(ADP-ribosyl)ation (PARylation) of VISA. This modification of VISA serves as a signal for the E3 ubiquitin ligase Ring figure protein 146 (RNF146), which polyubiquitinates VISA and leads to its degradation. Our findings reveal a mechanism for attenuating innate immune response to RNA viruses by the TNKS–RNF146 axis, which could help the development of drugs or vaccines against RNA virus infection.

Innate immunity presents the first line of host defense against microbial infection. Upon viral infection, virus-associated molecules, such as viral nucleic acids, are recognized by host germline-encoded pattern recognition receptors, which trigger a myriad of cellular signaling cascades that culminate in the transcription of the effector genes, including type I interferons (IFNs) and proinflammatory cytokines, to inhibit the virus infection and clear the infected cells (1).

Pathogen-derived RNA in the cytosol could be detected by retinoic acid–inducible gene-I–like receptors (RLRs), including by retinoic acid–inducible gene-I (RIG-I) and melanoma differentiation-associated gene 5 (MDA5). Although it has been well established that RIG-I and MDA5 have distinct specificities to different types of viruses, both RIG-I and MDA5 signal through the central adaptor protein VISA (virus-induced signal adaptor; also known as mitochondrial antiviral signaling protein (MAVS), CARD adaptor inducing IFN-β (Cardif), and interferon-beta promoter stimulator 1 (IPS-1) (2–5). VISA contains a C-terminal transmembrane (TM) domain that targets it to the outer membrane of mitochondria and an N-terminal Caspase recruitment domain (CARD) that is responsible for the recruitment of RLRs. Upon interaction with RLRs, VISA forms prion-like filaments and recruits several tumor necrosis factor receptor–associated factor (TRAF) proteins, including TRAF2, TRAF3, TRAF5, and TRAF6, through its TRAF-binding motif between the CARD and TM domain. Recruitment of TRAF proteins by VISA activates the downstream cytosolic kinases TBK1 and IKKs followed by the phosphorylation and nucleus translocation of the transcriptional factors IRF3/7 and nuclear factor-kappaB (NF-κB), thus inducing the transcription of downstream antiviral genes (6, 7).

Studies of VISA-deficient mice indicated that VISA not only plays a pivotal role in innate antiviral response but is also involved in the coordination of apoptotic and metabolic functions (8). Therefore, the activity and stability of VISA are tightly and delicately regulated to exert an optimal protective immune response and to avoid tissue damages and excessive harmful immune diseases. It has been well established that VISA is dynamically

Author contributions: C.-Q.L. designed research; Y.-R.X., M.-L.S., Y.Z., and C.-Q.L. performed research; N.K., C.W., Y.-F.X., and Q.-Y.Z. contributed new reagents/analytic tools; Y.-R.X., M.-L.S., Y.Z., Q.-Y.Z., and C.-Q.L. analyzed data; and Y.Z., S.-S.D., and C.-Q.L. wrote the paper.

The authors declare no competing interest.

This article is a PNAS Direct Submission.

[1]Y.-R.X., M.-L.S., and Y.Z. contributed equally to this work.

[2]To whom correspondence may be addressed. Email: caoqilei@whu.edu.cn.

This article contains supporting information online at http://www.pnas.org/lookup/suppl/doi:10.1073/pnas.2122805119/-/DCSupplemental.

Published June 21, 2022.

controlled by various forms of posttranslational modifications (PTMs). For example, the E3 ligase tripartite motif protein 31 (TRIM31) mediates the K63-linked polyubiquitination of VISA at lysine (K) 10/311/461, which promotes its aggregation and activation after virus infection (9). On the other hand, Ring figure protein 34 (RNF34) initiates the K63- to K27-linked polyubiquitination transition on K311 of VISA, leading to its degradation through autophagosome (10). A series of E3 ligases, including RNF125, TRIM25, RNF5, membrane-associated RING-CH 5 (MARCH5), SMAD specific E3 ubiquitin protein ligase1/2 (Smurf1/2), and atrophin-1–interacting protein 4 (AIP4), catalyzes K48-linked polyubiquitination and degradation of VISA, thereby shutting down the innate antiviral response (11–18), whereas the deubiquitinase ovarian tumor family deubiquitinase 4 (OTUD4) removes K48-linked ubiquitin moieties from VISA and maintains its stability after virus infection (19). In addition, VISA can also be phosphorylated by TBK1 and IKKβ upon virus infection; activated VISA then recruits IRF3 for its phosphorylation by TBK1 (20). By contrast, the protein phosphatase PPM1A (also known as PP2Gα) directly dephosphorylates VISA and impairs innate immune response at the late phase of virus infection (21). The protein kinase A catalytic subunits-α and -β phosphorylate VISA at Thr54, which impairs its aggregation and primes it for MARCH5-mediated polyubiquitination and degradation, thus attenuating innate antiviral response (22). More recently, *O*-linked β-*N*-acetylglucosamine (O-GlcNAc) transferase is reported to mediate O-GlcNAcylation of VISA on Ser366 following virus infection, which is a prerequisite for K63-linked polyubiquitination and activation of VISA (23). In addition, the protein arginine methyltransferase 7 catalyzes VISA monomethylation and suppresses VISA aggregation and activation (24). However, whether other forms of PTM regulate VISA-mediated innate antiviral response is unknown.

Adenosine diphosphate (ADP) ribosylation is a reversible PTM catalyzed by a group of polyadenosine diphosphate ribose polymerases (PARPs). PARPs conjugate a single ADP ribose moiety or polymers of ADP ribose moieties from nicotinamide adenine dinucleotide (NAD^+) to a variety of amino acid residues of target proteins, leading to Mono(ADP-ribosyl)ation (MARylation) or Poly(ADP-ribosyl)ation (PARylation) of the substrates. As a result, the PARP family, which is composed of 17 members, can be categorized according to their catalytic activities: "mono," "poly," or "inactive" (25). Although ADP ribosylation is best known for its roles in gene regulation and DNA damage repair, ADP ribose is found in both the nucleus and the cytoplasm. Recent studies have revealed an important role of ADP ribosylation in diverse cellular signaling pathways, including those in innate immune and inflammatory responses. For example, PARP7 suppresses TBK1 activity by mediating MARylation of TBK1 (26). PARP11 inhibits the type I IFN–induced signaling by MARylating the E3 ubiquitin ligase β-transducin repeats–containing protein (β-TrCP) (27). Moreover, PARP10 negatively regulates tumor necrosis factor α (TNFα)– and interleukin-1β (IL-1β)–induced NF-κB activation by mediating MARylation of NF-κB essential modulator (NEMO) (28). PARP9 and PARP13, which have no ADP ribosylation activity, inhibit viral replication through regulating the expression of some antiviral genes or directly targeting specific viral RNA (29–31). However, whether other PARPs, especially those capable of mediating PARylation of target proteins, regulate innate antiviral response remains to be determined.

Tankyrase 1 (TNKS1)/PARP5a and its homolog TNKS2/PARP5b are known to mediate PARylation of their substrates, which are implicated in diverse cellular processes, including telomere homeostasis, glucose metabolism, mitotic spindle formation, and WNT signaling (32). Both TNKS1 and TNKS2 harbor an N-terminal ankyrin repeat (ANK) responsible for binding target proteins that contain a TNKS-binding motif RxxxxG. TNKS1 and TNKS2 also contain a middle sterile alpha motif (SAM) domain that mediates their multimerization and a catalytic domain in the C terminus, which PARylates themselves or their binding partners (33). TNKS has been reported to regulate telomere homeostasis, WNT signaling, and tumor growth by PARylating and destabilizing TRF1, AXIN1/2, and PTEN, respectively (34–36).

In the present study, we identified VISA as a substrate for TNKS by the tandem affinity purification followed by mass spectrometry (TAP-MS) strategy. We found that viral infection led to the induction of TNKS1 and TNKS2, which translocated from cytosol to mitochondria and interacted with VISA. TNKS1 and TNKS2 then mediated PARylation of VISA, which primed it for K48-linked polyubiquitination by the E3 ligase RNF146 and led to its degradation. As a consequence, knockdown or knockout of TNKS1, TNKS2, or RNF146 potentiated RNA virus–triggered expression of downstream antiviral genes and impaired virus replication. In addition, either TNKS1 or TNKS2 deficiency promoted antiviral innate immune responses in mice. Collectively, our findings demonstrate that PARylation of VISA by TNKS1 and TNKS2 is a strategy by which the host controls excessive and harmful immune response.

Results

Identification of VISA as a TNKS Substrate. VISA is a critical adaptor protein in RNA virus–triggered innate immune response. To identify potential molecules associated with VISA, we generated HEK293 cells stably expressing SFB (S protein, Flag, and streptavidin-binding peptide)-tagged human VISA. Following a tandem affinity purification scheme, proteins associated with VISA were identified by mass spectrometry. By comparing with other unrelated purifications with the same strategy, we identified a series of proteins specifically associated with VISA (Fig. 1*A*). Among them, PCBP1, NLRX1, TRAF2, TRAF6, and PLK1 have been reported to be associated with VISA and involved in innate antiviral response (37), suggesting that the approach was effective in identifying VISA-associated proteins. Interestingly, the poly-ADP ribosyltransferase TNKS1 was also identified in the screening (Fig. 1*A*). To confirm the association of TNKS1 and VISA, we performed transient transfection and coimmunoprecipitation (Co-IP) experiments. The results indicated that TNKS1 interacted with VISA but not other tested proteins, including RIG-I, MDA5, cyclic GMP-AMP synthase (cGAS), mediator of IRF3 activation (MITA), TBK1, IKKβ, IRF3, and IRF7 (Fig. 1*B* and *SI Appendix*, Fig. S1*A*). Since TNKS2 is highly homologous with TNKS1, we tested if it would also associate with VISA. Co-IP experiments indicated that TNKS2 also interacted with VISA (Fig. 1*C* and *SI Appendix*, Fig. S1*B*). Furthermore, endogenous TNKS1 and TNKS2 were constitutively associated with low amounts of VISA in uninfected cells, and their association was further increased after Sendai virus (SeV) infection (Fig. 1*D*). These results confirm that TNKS1 and TNKS2 are VISA-associated proteins.

The interactions between TNKS1/2 and their substrates are usually mediated by their ANK region (33). Consistently, our domain mapping experiments indicated that the ANK region of TNKS1 and TNKS2 was required for their association with VISA (*SI Appendix*, Fig. S1 *C* and *D*). It has been reported that TNKS1 and TNKS2 recognize their substrates through a

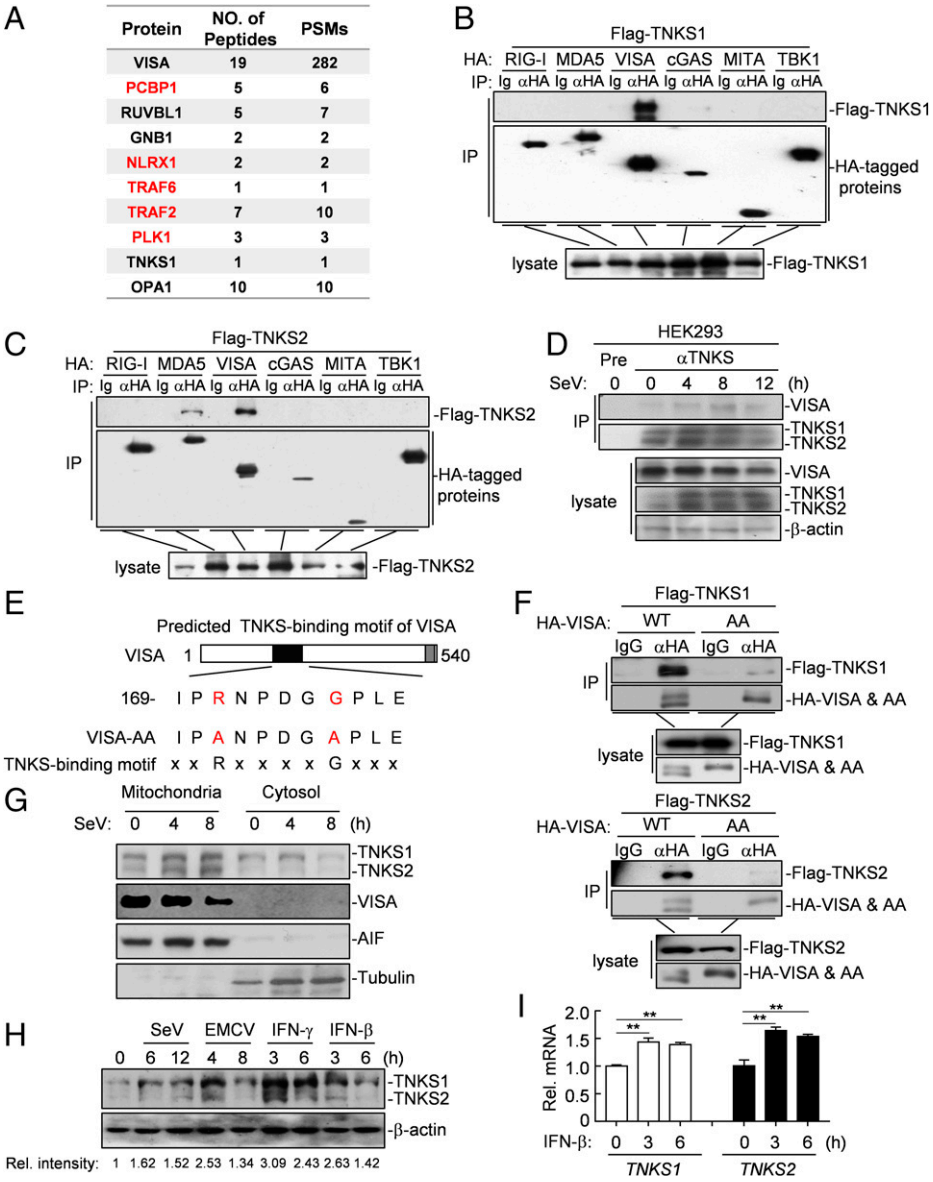

Fig. 1. Identification of TNKS as a VISA-associated protein. (*A*) HEK293 cells stably expressing SFB-tagged human VISA were subjected to TAP-MS experiments. The tables present summaries of the partial selected proteins identified by mass spectrometry analysis. (*B* and *C*) TNKS1 and TNKS2 interact with VISA. HEK293 cells (2×10^6) were transfected with the indicated plasmids for 20 h before Co-IP and immunoblotting analysis. (*D*) Endogenous TNKS1 and TNKS2 are associated with VISA. HEK293 cells (6×10^6) were untreated or infected with SeV for the indicated time points before Co-IP and immunoblotting analysis. (*E*) The schematic presentations of the wild-type and TNKS-binding motif mutant of VISA. (*F*) The TNKS-binding motif of VISA is required for its association with TNKS1 and TNKS2. HEK293 cells (2×10^6) were transfected with the indicated plasmids for 20 h before Co-IP and immunoblotting analysis. (*G*) Immunoblot analysis of the subcellular fractions. HEK293 cells (2×10^6) were untreated or infected with SeV for the indicated time points. Cell fractionations were performed, and the mitochondrial fraction (8%) and cytoplasm fraction (1.5%) were analyzed by immunoblotting with the indicated antibodies. (*H*) Induction of TNKS1 and TNKS2 by different stimuli. HEK293 cells were stimulated with SeV, EMCV, IFN-β (50 ng/mL), or IFN-γ (50 ng/mL) for the indicated time points before immunoblotting analysis. (*I*) IFN-β induced the transcription of *TNKS1* and *TNKS2*. HEK293 cells were stimulated with IFN-β (50 ng/mL) for the indicated time points before qRT-PCR analysis. Data are represented as the mean ± SEM. $^{**}P < 0.01$ (Student's *t* test). WT, wild type; AA, VISA-AA mutant; IP, immunoprecipitation; HA, hemagglutinin.

consensus RxxxxG motif (here referred to as the TNKS-binding motif) (33). Interestingly, we found that VISA contained a potential TNKS-binding motif (R^{171}NPDGG^{176}) at its N terminus (Fig. 1*E*). To determine whether this motif was responsible for its association with TNKS1 and TNKS2, we generated a VISA mutant (here referred to VISA-AA), in which the Arg171 and Gly176 were mutated to alanine (A) (Fig. 1*E*). Compared with wild-type VISA, VISA-AAs were dramatically impaired to interact with either TNKS1 or TNKS2 (Fig. 1*F*). Taken together, these results demonstrate that TNKS1 and TNKS2 interact with the TNKS-binding motif of VISA through their ANK region.

We next analyzed the subcellular localizations of TNKS1 and TNKS2. Cellular fractionation assays showed that both TNKS1 and TNKS2 were detectable in the mitochondrial and cytosol fractions in the absence of viral infection, and SeV infection induced the translocation of a fraction of TNKS1 and TNKS2 from cytosol to mitochondria (Fig. 1*G*). Confocal microscopy indicated that Flag-tagged TNKS1 and TNKS2 were partially colocalized with the mitochondria marker TOM20 (*SI Appendix*, Fig. S1*E*). Interestingly, we repeatedly observed that the protein levels of TNKS1 and TNKS2 were increased in HEK293 cells after SeV infection (Fig. 1 *D* and *G*). Therefore, we determined whether virus infection led to the induction of TNKS1 and TNKS2. As shown in Fig. 1*H*, the expressions of TNKS1 and TNKS2 were markedly induced by SeV, encephalomyocarditis virus (EMCV), IFN-β, or IFN-γ. qRT-PCR analysis showed that IFN-β induced about 1.5-fold induction of the messenger RNA (mRNA) level of *TNKS1* and *TNKS2* genes (Fig. 1*I*). Taken together, these results suggest that viral infection up-regulates the expressions of TNKS1 and TNKS2, which translocate to the mitochondria and interact with VISA.

TNKS1 and TNKS2 Negatively Regulate RNA Virus–Triggered Signaling. Because viral infection caused recruitment of TNKS1 and TNKS2 to the mitochondria and induced their association with VISA, we determined whether TNKS1 and TNKS2 regulated RNA virus–triggered innate immune signaling. As shown in *SI Appendix*, Fig. S2*A*, overexpression of TNKS1 or TNKS2 inhibited SeV-triggered activation of the IFN-β promoter in HEK293 cells. However, neither TNKS1 nor TNKS2 had a significant effect on IFN-γ–triggered activation of the IRF1 promoter (*SI Appendix*, Fig. S2*B*), indicating that TNKS1 and TNKS2 specifically regulated virus-triggered signaling. To

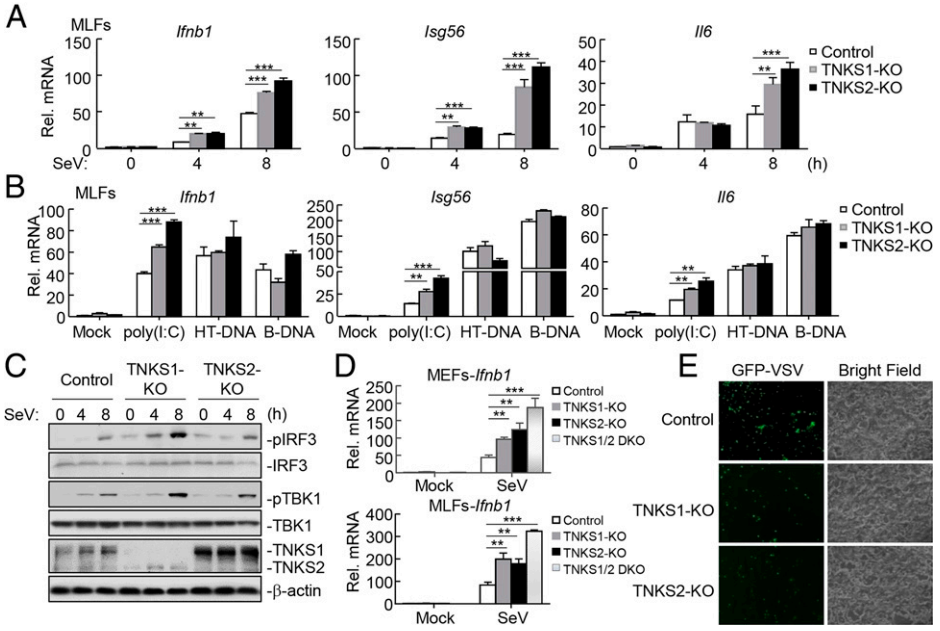

Fig. 2. TNKS1 and TNKS2 negatively regulate virus-triggered signaling. (*A*) Effects of TNKS1 or TNKS2 deficiency on the SeV-triggered transcription of downstream genes in MLFs. TNKS1- or TNKS2-deficient MLFs were generated by the CRISPR-Cas9 system. Then, the TNKS1-KO, TNKS2-KO, and control MEFs or MLFs (2×10^5) were untreated or infected with SeV for the indicated time points before qRT-PCR analysis. (*B*) Effects of TNKS1 or TNKS2 deficiency on the cytoplasmic transfected synthetic RNA- or DNA-triggered transcription of downstream genes. The TNKS1-KO, TNKS2-KO, and control MLFs (2×10^5) were untreated or transfected with poly(I:C), HT-DNA, or B-DNA for 10 h before qRT-PCR analysis. (*C*) Effects of TNKS1 or TNKS2 deficiency on the SeV-triggered phosphorylation of TBK1 and IRF3. The TNKS1-KO, TNKS2-KO, and control MLFs (4×10^5) were untreated or infected with SeV for the indicated time points before the immunoblotting analysis. (*D*) Effects of TNKS1 or TNKS2 double deficiency on the SeV-triggered transcription of *Ifnb1* gene in MEFs and MLFs. The TNKS1-KO, TNKS2-KO, TNKS1/2-DKO, and control MEFs or MLFs (2×10^5) were untreated or infected with SeV for the indicated time points before qRT-PCR analysis. (*E*) Effects of TNKS1 or TNKS2 deficiency on the replication of GFP-VSV. The TNKS1-KO, TNKS2-KO, and control MLFs (2×10^5) were infected with GFP-VSV for 24 h and imaged by microscopy. Data are represented as the mean ± SEM. $^{**}P < 0.01$ (Student's *t* test); $^{***}P < 0.001$ (Student's *t* test).

determine the roles of endogenous TNKS1 and TNKS2 in virus-triggered signaling, we constructed three TNKS1 and TNKS2 RNA interference (RNAi) plasmids, which dramatically reduced the expression of TNKS1 and TNKS2, respectively (*SI Appendix*, Fig. S2*C*). In reporter assays, knockdown of either TNKS1 or TNKS2 significantly potentiated SeV-triggered activation of the IFN-β promoter (*SI Appendix*, Fig. S2*D*) (we selected TNKS1-RNAi-#1 and TNKS2-RNA-#2 constructs for subsequent experiments), and simultaneous knockdown of both TNKS1 and TNKS2 markedly enhanced the potentiation effects on SeV- or the double-stranded RNA (dsRNA) analog polyinosinic:polycytidylic acid [poly(I:C)]–induced activation of the IFN-β promoter in comparison with knockdown of each of them alone (*SI Appendix*, Fig. S2*E*). In agreement with this, knockdown of either TNKS1 or TNKS2 markedly enhanced the SeV-triggered phosphorylation of TBK1 and IRF3, which are the prerequisites for the IFN-β promoter activation, and simultaneous knockdown of both TNKS1 and TNKS2 resulted in a further increase (*SI Appendix*, Fig. S2*F*). By contrast, knockdown of neither TNKS1 nor TNKS2 affected IFN-γ–triggered activation of the IRF1 promoter (*SI Appendix*, Fig. S2*G*). Together, these results indicate that TNKS1 and TNKS2 are negative regulators of virus-triggered innate immune signaling.

To further confirm the roles of TNKS1 and TNKS2 in virus trigger innate immune signaling, we generated TNKS1-knockout (TNKS1-KO) and TNKS2-deficient (TNKS2-KO) mouse embryonic fibroblasts (MEFs), mouse lung fibroblasts (MLFs), and HEK293 cells by the CRISPR-Cas9 system. qRT-PCR analysis showed that either TNKS1 or TNKS2 deficiency increased SeV-induced transcription of downstream effector genes, including *Ifnb1*, *Isg56*, and *Il6*, in MEFs, MLFs, and HEK293 cells (Fig. 2*A* and *SI Appendix*, Fig. S2 *H* and *I*). In addition, TNKS1 or TNKS2 deficiency also potentiated the transcription of *Ifnb1*, *Isg56*, and *Il6* induced by cytoplasmic transfection of poly(I:C) but not herring testis DNA (HT-DNA) or B-form DNA (B-DNA) (Fig. 2*B*). By contrast, neither TNKS1 nor TNKS2 deficiency affected IFN-γ–induced transcription of *IRF1*, *GBP2*, and *STAT1* in HEK293 cells and MLFs (*SI Appendix*, Fig. S2*J*). Consistently, phosphorylation of TBK1 and IRF3 induced by SeV was markedly increased in TNKS1- or TNKS2-deficient MLFs compared with wild-type MLFs (Fig. 2*C*). We also generated TNKS1 and TNKS2 double-knockout (TNKS1/2 DKO) MEFs and MLFs by the CRISPR-Cas9 system and found that double knockout of TNKS1 and TNKS2 further increased SeV-induced transcription of the *Ifnb1* gene compared with TNKS1 or TNKS2 deficiency alone (Fig. 2*D*). We next determined whether TNKS1 and TNKS2 regulated antiviral responses during virus infection and infected TNKS1- or TNKS2-deficient and control MLFs with green fluorescent protein (GFP)–tagged vesicular stomatitis virus (VSV). As shown in Fig. 2*E*, replication of GFP-tagged VSV was markedly inhibited in TNKS1- or TNKS2-deficient cells compared with that in control cells as monitored by GFP signals. These results together suggest that TNKS1 and TNKS2 negatively regulate RNA virus– and cytosolic poly(I:C)–triggered innate immune signaling.

TNKS1 or TNKS2 Deficiency Enhances RNA Virus–Triggered Innate Immune Signaling in Mouse Primary Cells. To examine whether TNKS regulated virus-triggered innate immune signaling in primary immune cells, we first obtained $Tnks2^{fl/fl:Cre\text{-}ER+}$ mice by crossing $Tnks2^{fl/+}$ mice with ROSA26-CreERT2 (here referred to Cre-ER) mice, which carry a ubiquitous expressing Cre recombinase inducible by 4-hydroxytamoxifen (4-OHT). We prepared bone marrow–derived dendritic cells (BMDCs) and bone marrow–derived macrophages (BMDMs) from $Tnks2^{fl/fl}$ and $Tnks2^{fl/fl:Cre\text{-}ER+}$ mice. We next infected 4-OHT–treated $Tnks2^{fl/fl}$ and $Tnks2^{fl/fl:Cre\text{-}ER+}$ BMDCs and BMDMs

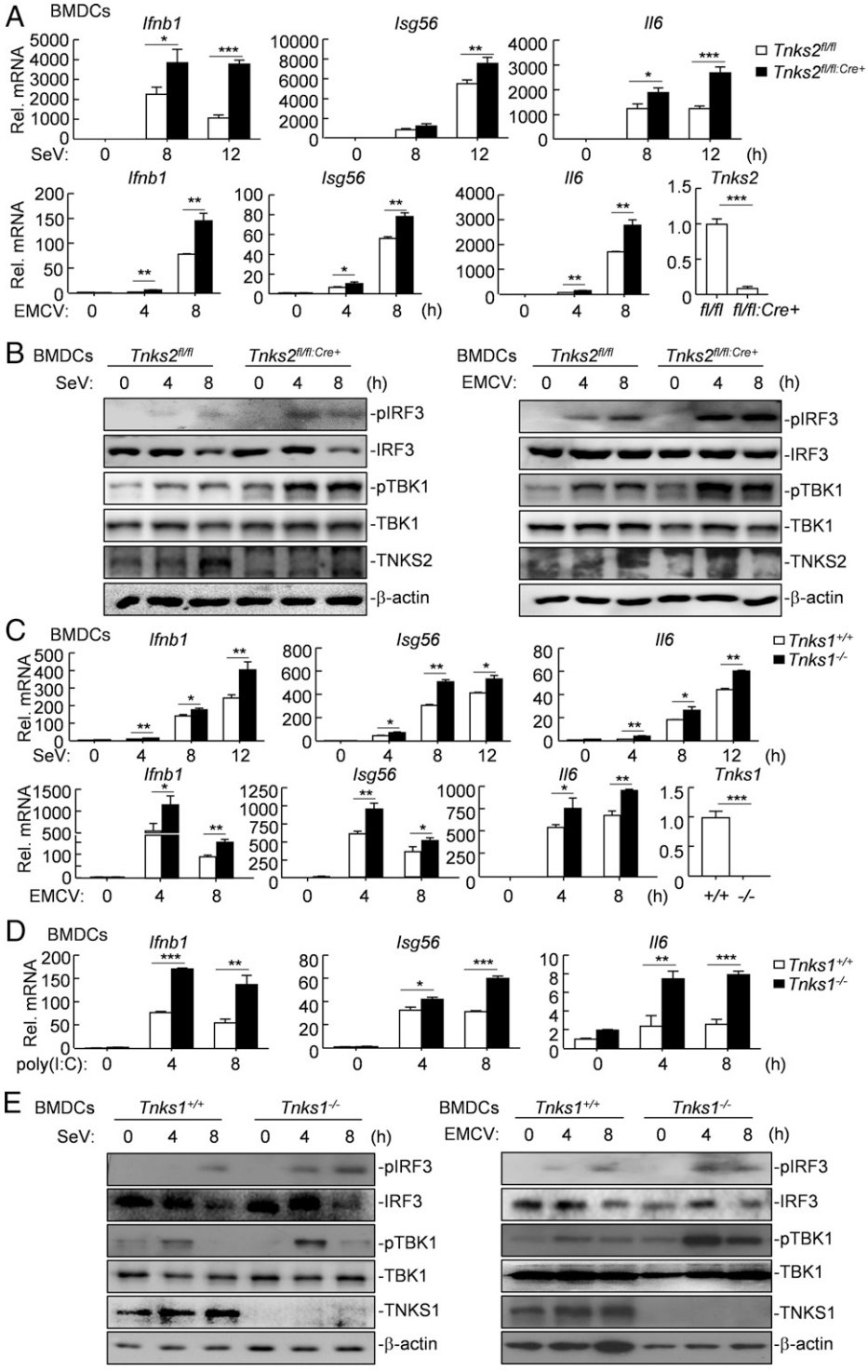

Fig. 3. TNKS1 or TNKS2 deficiency potentiates virus-triggered signaling in mouse primary cells. (*A*) Effects of TNKS2 deficiency on SeV- or EMCV-induced transcription of downstream genes in BMDCs. *Tnks2*$^{fl/fl}$ and *Tnks2*$^{fl/fl:Cre\text{-}ER+}$ BMDCs (2×10^5) were treated with 4-OHT (1 μM) for 3 d followed by infection with SeV or EMCV for the indicated time points before qRT-PCR analysis. (*B*) Effects of TNKS2 deficiency on SeV- or EMCV-induced phosphorylation of TBK1 and IRF3. *Tnks2*$^{fl/fl}$ and *Tnks2*$^{fl/fl:Cre\text{-}ER+}$ BMDCs (4×10^5) were treated with 4-OHT (1 μM) for 3 d followed by infection with SeV or EMCV for the indicated time points before immunoblotting analysis. (*C*) Effects of TNKS1 deficiency on SeV- or EMCV-induced transcription of downstream genes in BMDCs. *Tnks1*$^{+/+}$ and *Tnks1*$^{-/-}$ BMDCs (2×10^5) were left untreated or infected with SeV or EMCV for the indicated time points before qRT-PCR analysis. (*D*) Effects of TNKS1 deficiency on cytoplasmic transfected poly(I:C)-induced transcription of downstream genes in BMDCs. *Tnks1*$^{+/+}$ and *Tnks1*$^{-/-}$ BMDMs (2×10^5) were left untreated or transfected with poly(I:C) (1 μg) for the indicated time points before qRT-PCR analysis. (*E*) Effects of TNKS1 deficiency on SeV- or EMCV-induced phosphorylation of TBK1 and IRF3. *Tnks1*$^{+/+}$ and *Tnks1*$^{-/-}$ BMDCs (4×10^5) were left untreated or infected with SeV or EMCV for the indicated time points before immunoblotting analysis. Data are represented as the mean ± SEM. **P* < 0.05 (Student's *t* test); ***P* < 0.01 (Student's *t* test); ****P* < 0.001 (Student's *t* test).

with SeV or EMCV. qRT-PCR analysis indicated that TNKS2 deficiency potentiated transcriptions of downstream antiviral genes, including *Ifnb1*, *Isg56*, and *Il6*, induced by SeV or EMCV in BMDCs (Fig. 3*A*) and BMDMs (*SI Appendix*, Fig. S3*A*). In addition, phosphorylation of TBK1 and IRF3 induced by SeV or EMCV was markedly increased in *Tnks2*$^{fl/fl:Cre\text{-}ER+}$ compared with that of wild-type BMDCs (Fig. 3*B*). These data suggest that TNKS2 deficiency potentiates RNA virus–triggered induction of downstream antiviral genes in mouse primary immune cells.

We also prepared BMDCs and BMDMs from TNKS1-deficient and wild-type mice. qRT-PCR analysis indicated that TNKS1 deficiency significantly potentiated SeV- or EMCV-triggered transcription of downstream effector genes, including *Ifnb1*, *Isg56*, and *Il6*, in BMDCs (Fig. 3*C*) and BMDMs (*SI Appendix*, Fig. S3*B*). Moreover, transcription of *Ifnb1*, *Isg56*, and *Il6* induced by cytoplasmic transfection of poly(I:C) was enhanced in *Tnks1*$^{-/-}$ BMDCs compared with wild-type BMDCs (Fig. 3*D*). Consistently, phosphorylation of TBK1 and IRF3 induced by SeV or EMCV was increased in TNKS1-deficient BMDCs in comparison with wild-type BMDCs (Fig. 3*E*). Taken together, these results suggest that TNKS1 also attenuates virus-triggered innate immune signaling in mouse primary immune cells.

TNKS1 or TNKS2 Deficiency Promotes Innate Immune Response to RNA Virus in Mice. To characterize the roles of TNKS2 in vivo, we intraperitoneally injected *Tnks2*$^{fl/fl}$ and *Tnks2*$^{fl/fl:Cre\text{-}ER+}$ mice

with tamoxifen (80 μg/g) once every 24 h for a total of 5 d consecutively followed by a 7-d waiting period. qRT-PCR analysis indicated that intraperitoneal injection of tamoxifen led to efficient deletion of TNKS2 in all detected organs or tissues, including lung, liver, brain, muscle, heart, spleen, bone marrow–derived progenitor cells, and peripheral blood mononuclear cells (*SI Appendix*, Fig. S4*A*). Thus, the strategy to knock out TNKS2 in mice was reliable and successful. We next infected the tamoxifen-pretreated $Tnks2^{fl/fl}$ and $Tnks2^{fl/fl:Cre\text{-}ER+}$ mice with EMCV. As shown in Fig. 4*A*, the concentrations of IFN-β, IL-6, and MCP1 were significantly increased in the sera from $Tnks2^{fl/fl:Cre\text{-}ER+}$ mice compared with those from the $Tnks2^{fl/fl}$ mice after EMCV infection. The transcription of *Ifnb1* and *Isg56* was also significantly increased, and the replication of EMCV was impaired in the lungs and brains from $Tnks2^{fl/fl:Cre\text{-}ER+}$ mice compared with their control littermates after EMCV infection (Fig. 4*B*). Consistent with these observations, hematoxylin and eosin (H&E) staining analysis showed that there were more infiltrated immune cells in the lungs of $Tnks2^{fl/fl:Cre\text{-}ER+}$ mice than those of wild-type mice after EMCV infection (Fig. 4*C*). As a consequence, $Tnks2^{fl/fl:Cre\text{-}ER+}$ mice were more resistant to EMCV-induced death compared with their control littermates (Fig. 4*D*). Taken together, these results suggest that TNKS2 inhibits innate immune responses in mice.

We also examined the roles of TNKS1 in RNA virus infection in vivo and infected wild-type and $Tnks1^{-/-}$ mice with EMCV via intraperitoneal injection. Sera from $Tnks1^{-/-}$ mice infected with EMCV showed higher levels of IFN-β, IL-6, and MCP1 in comparison with those from their wild-type littermates (Fig. 4*E*). Moreover, the transcription of *Ifnb1* and *Isg56* was significantly increased, whereas the replication of EMCV was impaired in the lungs and brains from $Tnks1^{-/-}$ mice compared with those from $Tnks1^{+/+}$ mice after EMCV infection (Fig. 4*F*). H&E staining analysis indicated that EMCV infection induced more immune cells infiltration and caused severe damages in the lungs of $Tnks1^{-/-}$ mice compared with wild-type mice (Fig. 4*G*). We also monitored the survival of $Tnks1^{+/+}$ and $Tnks1^{-/-}$ mice every 12 h after EMCV infection. Unexpectedly, unlike the TNKS2-deficient mice, the $Tnks1^{-/-}$ mice were more susceptible to EMCV-induced death compared with the wild-type mice (Fig. 4*H*). This seemingly counterintuitive result prompted us to check the expression of *Tnks1* and *Tnks2* in different tissues of mice and examine the pathologic alterations in $Tnks1^{-/-}$ mice after viral infection. qRT-PCR analysis indicted that both *Tnks1* and *Tnks2* were abundantly expressed in the lung and heart but not the kidney. Interestingly, the expression of *Tnks1* was modest in the liver, but the expression of *Tnks2* was rather scarce in the liver (*SI Appendix*, Fig. S4*B*). In the absence of infection, the brains, lungs, hearts, spleens, and kidneys are comparable between $Tnks1^{+/+}$ and $Tnks1^{-/-}$ mice. Although the livers from $Tnks1^{-/-}$ mice were smaller compared with those from wild-type mice, the difference was not significant when normalized to the body weight (*SI Appendix*, Fig. S4*C*), which is consistent with a previous report (38). After infection with EMCV, the brains, lungs, hearts, spleens, and kidneys from $Tnks1^{+/+}$ and $Tnks1^{-/-}$ mice had a comparable appearance; however, the liver sizes were significantly reduced in $Tnks1^{-/-}$ mice compared with those from their wild-type littermates (*SI Appendix*, Fig. S4*C*). H&E staining indicated that the liver from TNKS1-deficient mice displayed more severe injury and typical centrilobular necrosis than that from wild-type mice post-EMCV infection (*SI Appendix*, Fig. S4*D*). We also infected $Tnks1^{+/+}$ and $Tnks1^{-/-}$ mice with influenza virus A/Puerto Rico/8/1934 (H1N1) (PR8) through intranasal inhalation. Compared with wild-type mice, $Tnks1^{-/-}$ mice showed higher levels of IFN-β, IL-6, and MCP1 in the sera (*SI Appendix*, Fig. S4*E*). Similar to the phenotypes of $Tnks1^{-/-}$ mice infected with EMCV, $Tnks1^{-/-}$ mice infected with influenza virus PR8 also suffered more sever liver damage (*SI Appendix*, Fig. S4*F*) and were more susceptible to PR8-induced death (*SI Appendix*, Fig. S4*G*). By contrast, the size of the liver and the pathological alterations were comparable between TNKS2-deficient and wild-type mice (*SI Appendix*, Fig. S4 *H* and *I*). These results suggest that TNKS1 negatively regulates innate antiviral responses in vivo and may have important functions in the liver; however, TNKS1-deficient mice exhibit early death after virus infection, which may be due to severe liver damages.

TNKS1 and TNKS2 Mediate VISA PARylation and Promote Its Degradation. TNKS1 and TNKS2 are enzymes that catalyze PARylation of their substrates; we thus determined whether their enzymatic activity was required for the regulation of innate antiviral responses. AZ6102, JW55, and XAV939 are three potent inhibitors for PARP activity of TNKS, which significantly potentiated SeV-triggered transcription of *Ifnb1* in MLFs (Fig. 5*A*). Moreover, we found that wild-type TNKS1 and TNKS2 but not their PARP-dead mutants TNKS1-PD or TNKS2-PD reduced SeV-triggered transcription of *IFNB1* (Fig. 5*B*). These results indicate that the enzymatic activity of TNKS is indispensable for their inhibitory effects on virus-triggered induction of downstream genes. Because TNKS1 and TNKS2 were associated with VISA, we next examined whether TNKS1 and TNKS2 function through VISA. In reporter assays, knockdown of either TNKS1 or TNKS2 potentiated activation of the IFN-β promoter mediated by RIG-I or VISA but had minor effects on the activation of the IFN-β promoter mediated by cGAS-MITA or TBK1 (*SI Appendix*, Fig. S5 *A* and *B*). Thus, TNKS1 and TNKS2 regulate innate antiviral response via VISA.

Having established that TNKS1 and TNKS2 interacted with VISA and that the enzymatic activity was required for the inhibitory effects on virus-triggered signaling, we investigated whether TNKS1 and TNKS2 PARylated VISA. As shown in Fig. 5*C*, overexpression of either TNKS1 or TNKS2 resulted in the PARylation of VISA, whereas overexpression of TNKS1-PD did not mediate the PARylation of VISA (Fig. 5*D*). To confirm that TNKS1 and TNKS2 directly PARylated VISA, we performed an in vitro ribosylation assay as illustrated in Fig. 5 *E*, *Upper* and found that recombinant *Escherichia coli*–derived His-VISA protein could be PARylated by TNKS1 and TNKS2 but not their enzymatic-inactive mutants (Fig. 5 *E*, *Lower*). We further examined the PARylation of endogenous VISA in the absence or presence of viral infection. As shown in Fig. 5*F*, VISA was weakly PARylated in uninfected cells, and SeV infection increased PARylation of VISA, which peaked at 6 h after infection. However, TNKS1 or TNKS2 deficiency dramatically inhibited SeV-triggered PARylation of VISA. Taken together, these results suggest that TNKS1 and TNKS2 directly mediate the PARylation of VISA.

Since PARylation of some TNKS substrates is known to lead to their degradation (39), we determined whether TNKS1 and TNKS2 affected the stability of VISA. As shown in Fig. 5*G*, the expression of VISA was dramatically down-regulated by TNKS1 and TNKS2 but not their enzymatic-inactive mutants. Conversely, TNKS1 or TNKS2 deficiency markedly inhibited SeV-trigged degradation of VISA compared with the control HEK293 cells (Fig. 5*F*). Similarly, TNKS1 or TNKS2 deficiency also slowed the SeV-triggered degradation of VISA in BMDCs (Fig. 5*H*). By contrast, TNKS1 or TNKS2 deficiency did not affect the

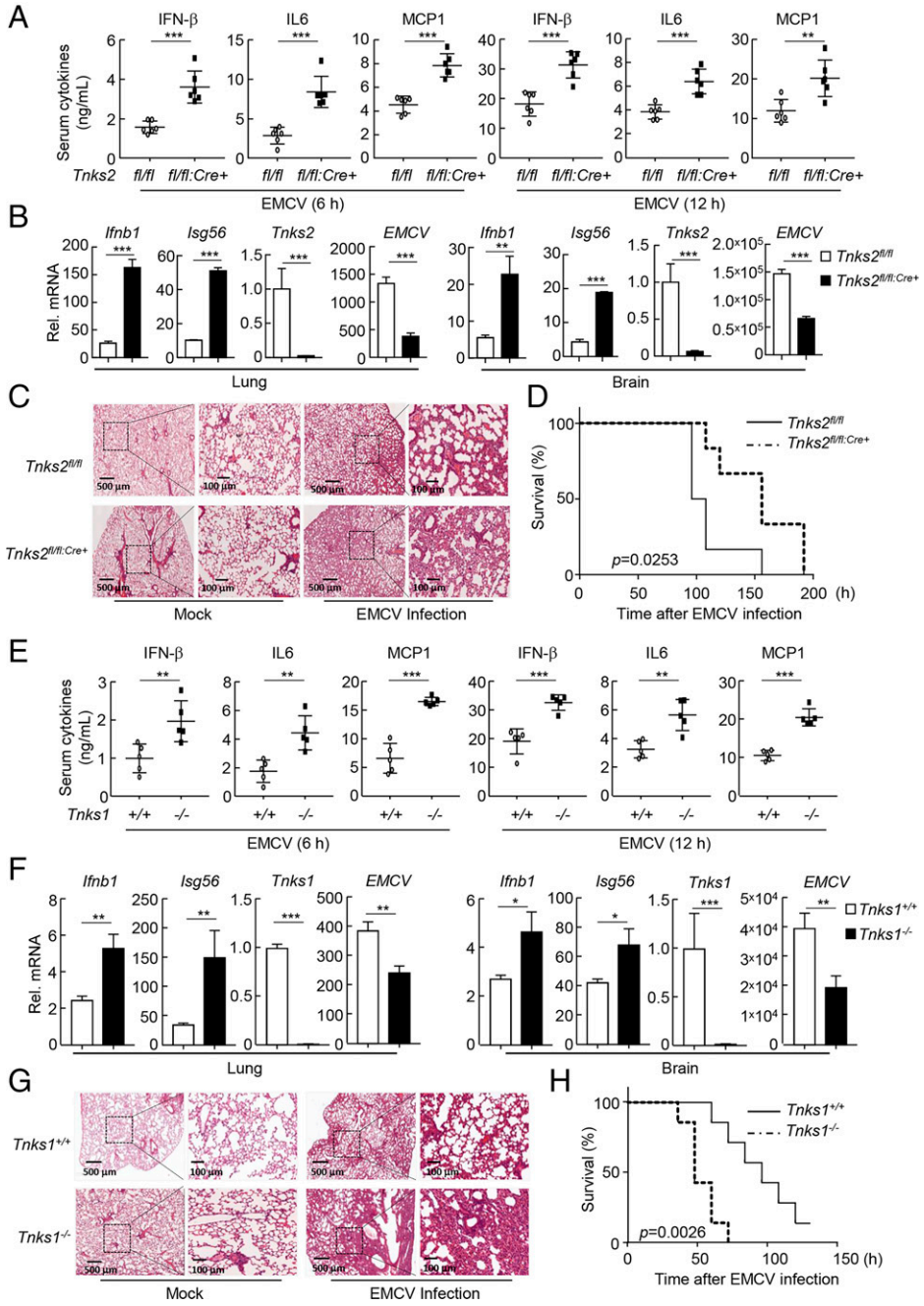

Fig. 4. TNKS1 and TNKS2 deficiency potentiates innate immune and inflammatory responses in mice. (*A*) Effects of TNKS2 deficiency on serum levels of IFN-β, IL-6, and MCP1 induced by EMCV infection. Sex- and age-matched *Tnks2*$^{fl/fl}$ and *Tnks2*$^{fl/fl:Cre\text{-}ER+}$ mice ($n = 6$) were injected intraperitoneally with tamoxifen (80 μg/g dissolved in corn oil) for 5 d consecutively, and 7 d later, the mice were intraperitoneally injected with EMCV (1×10^8 PFU per mouse) for the indicated time points before measurement of the indicated serum cytokines by ELISA. Each symbol represents an individual mouse. (*B*) qRT-PCR analysis of *Ifnb1*, *Isg56*, and *EMCV-gp2* or *Tnks2* in the lungs and brains from *Tnks2*$^{fl/fl}$ and *Tnks2*$^{fl/fl:Cre\text{-}ER+}$ mice. *Tnks2*$^{fl/fl}$ and *Tnks2*$^{fl/fl:Cre\text{-}ER+}$ mice were pretreated as described in *A* and were further intraperitoneally injected with EMCV (1×10^8 PFU per mouse) for 3 d; the lungs and brains were retrieved for qRT-PCR analysis. (*C*) H&E staining of lungs from *Tnks2*$^{fl/fl}$ and *Tnks2*$^{fl/fl:Cre\text{-}ER+}$ mice. *Tnks2*$^{fl/fl}$ and *Tnks2*$^{fl/fl:Cre\text{-}ER+}$ mice were pretreated as described in *A* and were further intraperitoneally injected with EMCV (1×10^8 PFU per mouse) for 3 d; the lungs of mice were analyzed by histology with H&E staining. (*D*) Effects of TNKS2 deficiency on EMCV-induced death. *Tnks2*$^{fl/fl}$ and *Tnks2*$^{fl/fl:Cre\text{-}ER+}$ mice were pretreated as described in *A* and were further intraperitoneally injected with EMCV (1×10^8 PFU per mouse, $n = 6$ for each genotype group); mouse survival was observed and recorded every 12 h. (*E*) Effects of TNKS1 deficiency on serum levels of IFN-β, IL-6, and MCP1 induced by EMCV infection. Sex- and age-matched *Tnks1*$^{+/+}$ and *Tnks1*$^{-/-}$ mice ($n = 5$) were injected intraperitoneally with EMCV (1×10^8 PFU per mouse) for the indicated time points before measurement of the indicated serum cytokines by ELISA. Each symbol represents an individual mouse. (*F*) qRT-PCR analysis of *Ifnb1*, *Isg56*, and *EMCV-gp2* or *Tnks1* in the lungs and brains from *Tnks1*$^{+/+}$ and *Tnks1*$^{-/-}$ mice. Sex- and age-matched *Tnks1*$^{+/+}$ and *Tnks1*$^{-/-}$ mice ($n = 5$) were injected intraperitoneally with EMCV (1×10^8 PFU per mouse) for 3 d, and the lungs and brains were retrieved for qRT-PCR analysis. (*G*) H&E staining of the lungs from *Tnks1*$^{+/+}$ and *Tnks1*$^{-/-}$ mice. Sex- and age-matched *Tnks1*$^{+/+}$ and *Tnks1*$^{-/-}$ mice ($n = 5$) were left untreated or injected intraperitoneally with EMCV (1×10^8 PFU per mouse) for 3 d, and the lungs of mice were analyzed by histology with H&E staining. (*H*) Effects of TNKS1 deficiency on EMCV-induced death. Sex- and age-matched *Tnks1*$^{+/+}$ and *Tnks1*$^{-/-}$ mice were infected intraperitoneally with EMCV (1×10^8 PFU per mouse, $n = 7$), and mouse survival was observed and recorded every 12 h. Data are represented as the mean ± SEM. *$P < 0.05$ (Student's *t* test); **$P < 0.01$ (Student's *t* test); ***$P < 0.001$ (Student's *t* test). PFU, plaque-forming units; ELISA, enzyme linked immunosorbent assay.

transcription of *Visa* (*SI Appendix*, Fig. S5*C*). In addition, the level of VISA-AA, which was impaired for interaction with TNKS1 and TNKS2, was not reduced by overexpression of TNKS1 or TNKS2 (*SI Appendix*, Fig. S5*D*). Collectively, these results suggest that both TNKS1 and TNKS2 inhibit innate immune response by PARylating VISA, which lead to its degradation.

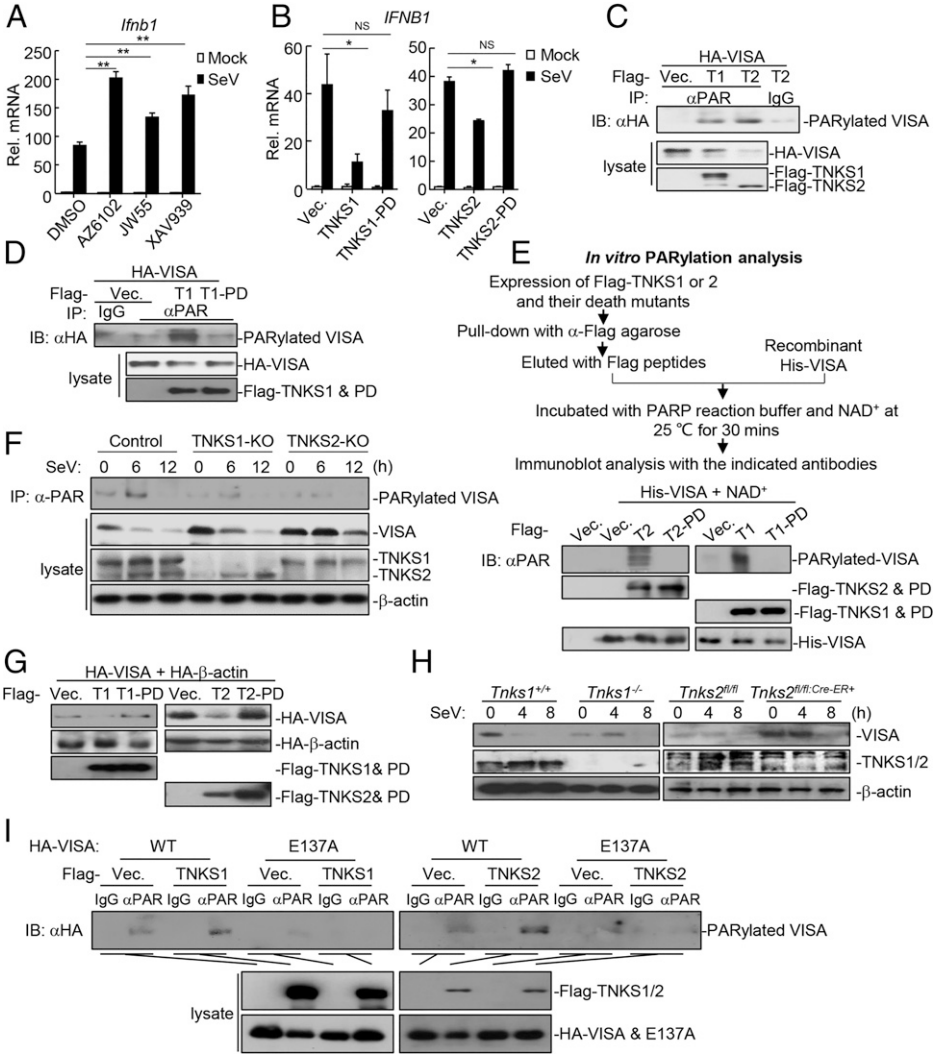

Fig. 5. TNKS1 and TNKS2 mediate PARylation and degradation of VISA. (*A*) Effects of TNKS inhibitors on virus-triggered transcription of *Ifnb1*. MLFs (2×10^5) were treated with dimethyl sulfoxide (DMSO) or the indicated TNKS inhibitors (10 μM) for 48 h, and the cells were then untreated or infected with SeV for 6 h before qRT-PCR analysis. (*B*) Effects of TNKS1, TNKS2, and their enzymatic-inactive mutants on the SeV-triggered transcription of *IFNB1*. HEK293 cells (2×10^5) were transfected with the indicated plasmids for 24 h, and the cells were then untreated or infected with SeV for 10 h before qRT-PCR analysis. (*C*) TNKS1 and TNKS2 mediate PARylation of VISA. HEK293 cells (2×10^6) were transfected with the indicated plasmids for 24 h; then, the cell lysates were immunoprecipitated with anti-PAR or IgG antibodies for 4 h, and the immunoprecipitates were analyzed by immunoblotting analysis with anti-HA. The expression levels of the related proteins were detected by immunoblotting analysis with the indicated antibodies. T1, TNKS1; T2, TNKS2. (*D*) Effects of TNKS1 or TNKS1-PD on the PARylation of VISA. The experiments were performed as described in *C*. T1, TNKS1. (*E*) TNKS1 and TNKS2 mediate PARylation of VISA in vitro. HEK293 cells were transfected with Flag-tagged TNKS1, TNKS2, and their mutants for 24 h. The cells were lysed and immunoprecipitated with anti-Flag for 2 h at 4 °C; the beads were then washed and eluted with FLAG peptide followed by incubation with purified His-VISA in PARP reaction buffer in the presence of NAD^+ at 25 °C for 30 min. Reactions were terminated by the addition of 2× sodium dodecyl sulfate (SDS) loading buffer, and the samples were then detected by immunoblotting analysis with the indicated antibodies. T1, TNKS1; T2, TNKS2. (*F*) Effects of TNKS1 or TNKS2 deficiency on the PARylation of VISA. The TNKS1 or TNKS2 deficiency and control HEK293 cells (6×10^6) were untreated or infected with SeV for the indicated time points; then, the cell lysates were immunoprecipitated with anti-PAR for 6 h, and the immunoprecipitates were analyzed by immunoblot with anti-VISA. The expression levels of the related proteins were detected by immunoblotting analysis with the indicated antibodies. (*G*) Effects of TNKS1, TNKS2, and their enzymatic-inactive mutants on the expression of VISA. HEK293 cells (2×10^5) were transfected with the indicated plasmids for 24 h, and the cells were then analyzed by immunoblotting analysis. T1, TNKS1; T2, TNKS2. (*H*) TNKS1 or TNKS2 deficiency inhibits SeV-triggered VISA degradation. The wild-type and TNKS1- or TNKS2-deficient BMDCs (4×10^5) were left untreated or infected with SeV for the indicated time points before immunoblotting analysis. (*I*) TNKS1 and TNKS2 catalyze the PARylation of VISA at E137. The experiments were performed as described in *C*. Data are represented as the mean ± SEM. NS, no significance. $^*P < 0.05$ (Student's *t* test); $^{**}P < 0.01$ (Student's *t* test). IP, immunoprecipitation; HA, hemagglutinin; IgG, immunoglobulin G; Vec, vector; WT, wild type; E137A, VISA-E137A mutant.

It has been reported that ADP ribosylation occurred predominantly on glutamic (E) and aspartic (D) acid residues (40, 41). To identify the potential PARylation residues of VISA, we mutated all of the 33 Glu residues and 20 Asp residues of VISA to alanine individually and examined whether these mutants could be inhibited by TNKS by monitoring IFN-β activation. Thus, we found that TNKS2 inhibited IFN-β activation mediated by all the VISA mutants but not VISA-E137A (*SI Appendix*, Fig. S6*A*). Moreover, the levels of all tested VISA mutants except VISA-E137A were markedly down-regulated by TNKS2 (*SI Appendix*, Fig. S6*B*). Similar results were also obtained with TNKS1 (*SI Appendix*, Fig. S6 *C* and *D*). Consistent with this, PARylation assays indicated that overexpression of TNKS1 and TNKS2 resulted in the PARylation of wild-type VISA but not VISA-E137A (Fig. 5*I*). Taken together, these results suggest that TNKS1 and TNKS2 directly mediate PARylation of VISA at Glu137.

RNF146 Targets VISA for Polyubiquitination and Degradation. Previous studies have shown that the E3 ligase RNF146 recognizes PARylated TNKS substrates, including Axin, 3BP2, and PTEN (36, 39, 42), by binding to an internal unit of PAR through its WWE domain. This binding promotes the polyubiquitination and degradation of TNKS substrates (43). We thus examined whether RNF146 would recognize the PARylated VISA. As shown in Fig. 6*A*, RNF146 specifically interacted with VISA but not MDA5 or RIG-I in HEK293 cells, and this interaction was impaired by the TNKS inhibitors XAV939 and JW55 (Fig. 6*B*). In addition, RNF146 could not interact with VISA-AA, which lost its ability to interact with TNKS (Fig. 6*C*). These results suggested that PARylation of VISA by TNKS was required for RNF146 to interact with VISA. In support of this, domain mapping experiments indicated that the Trp–Trp–Glu (WWE) domain of RNF146, which has been shown to recognize the ADP ribosylated targets, was required for its association with VISA (Fig. 6*D*). Endogenous Co-IP experiments indicated that RNF146 was weakly associated with VISA in the absence of viral infection, and their association was dramatically increased after SeV infection (Fig. 6*E*). Collectively, these data suggested that RNF146 is physiologically associated with VISA, and this association could be further enhanced upon virus infection.

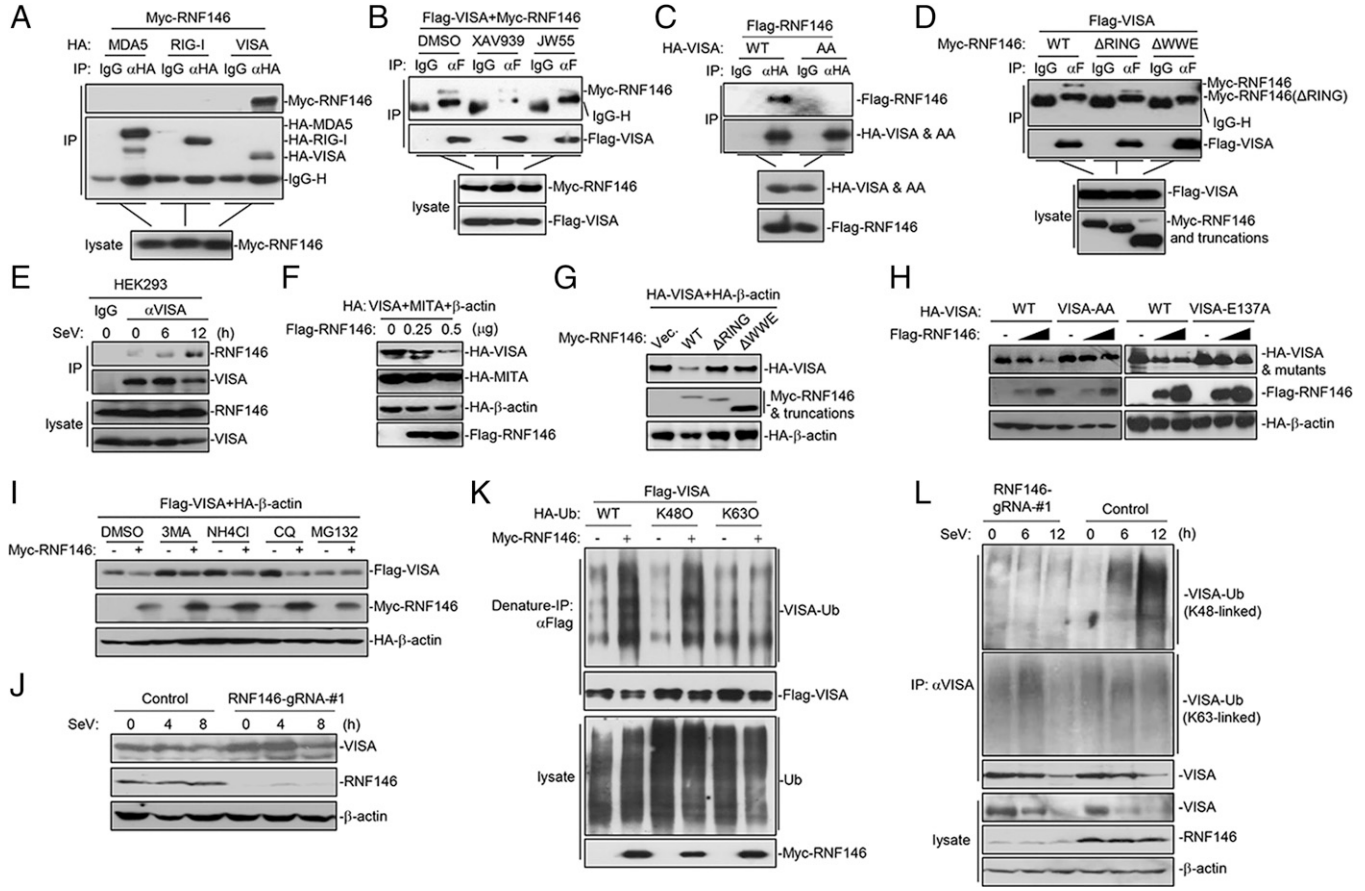

Fig. 6. RNF146 mediates polyubiquitination and degradation of VISA. (*A*) RNF146 interacts with VISA. HEK293 cells (2×10^6) were transfected with the indicated plasmids for 20 h before Co-IP and immunoblotting analysis. (*B*) Effects of TNKS inhibitors on the interaction between RNF146 and VISA. HEK293 cells (2×10^6) were transfected with the indicated plasmids for 20 h before Co-IP and immunoblotting analysis. (*C*) The TNKS-binding motif of VISA is required for its association with RNF146. HEK293 cells (2×10^6) were transfected with the indicated plasmids for 20 h before Co-IP and immunoblotting analysis. (*D*) RNF146 interacts with VISA through its WWE domain. HEK293 cells (2×10^6) were transfected with the indicated plasmids for 20 h before Co-IP and immunoblotting analysis. IgG-H is the heavy chain of IgG. (*E*) Endogenous RNF146 is associated with VISA. HEK293 cells (6×10^6) were untreated or infected with SeV for the indicated time points before Co-IP and immunoblotting analysis. (*F*) RNF146 inhibits the expression of VISA. HEK293 cells (2×10^5) were transfected with the indicated plasmids for 24 h, and the cells were then analyzed by immunoblotting analysis. (*G*) The RING domain and WWE domain of RNF146 are required for its inhibitory effects on the VISA expression. HEK293 cells (2×10^5) were transfected with the indicated plasmids for 24 h, and the cells were then analyzed by immunoblotting analysis. (*H*) RNF146 destabilizes the wild type but not VISA-AA or VISA-E137A. HEK293 cells (2×10^5) were transfected with the indicated plasmids for 24 h, and the cells were then analyzed by immunoblotting analysis. (*I*) RNF146 mediates VISA degradation in a proteasome-dependent manner. HEK293 cells (2×10^5) were transfected with the indicated plasmids for 24 h; the cells were then treated with the indicated inhibitors for 6 h before immunoblotting analysis. (*J*) The effects of RNF146 deficiency on the VISA expression. The RNF146-deficient and control HEK293 cells (4×10^5) were infected with SeV for the indicated time points; the cells were then analyzed by the immunoblotting analysis. (*K*) RNF146 mediates K48-linked polyubiquitination of VISA. HEK293 cells (2×10^6) were transfected with the Flag-VISA, HA-tagged ubiquitin (HA-Ub), ubiquitin K48-only (K48O), or K63-only (K63O) mutant with or without Myc-RNF146. Twenty-four hours later, the cell lysates were denatured and reimmunoprecipitated with anti-Flag; then, they were analyzed by immunoblotting with anti-HA (*Upper*). The expression levels of the proteins were analyzed by immunoblotting analysis with the indicated antibodies (*Lower*). (*L*) The effects of RNF146 deficiency on the SeV-induced polyubiquitination of VISA. HEK293 cells (6×10^6) were untreated or infected with SeV for the indicated time points; the cell lysates were then immunoprecipitated with anti-VISA for 6 h, and the immunoprecipitates and expression levels of the related proteins were analyzed by immunoblot with the indicated antibodies. CQ, chloroquine; DMSO, dimethyl sulfoxide; IP, immunoprecipitation; HA, hemagglutinin; IgG, immunoglobulin G; IgG-H, the heavy chain of IgG; WT, wild type; AA, VISA-AA.

We next determined whether RNF146 regulated the polyubiquitination and stability of VISA. As shown in Fig. 6*F*, overexpression of RNF146 down-regulated the level of VISA but not MITA in a dose-dependent manner. As expected, RNF146 mutants lacking the WWE domain or the RING domain, which is required for RNF146 to interact with VISA or its E3 ligase activity, failed to reduce the level of VISA (Fig. 6*G*). In agreement with this, RNF146 could not reduce the level of VISA-AA and VISA-E137A (Fig. 6*H*), indicating that the PARylation of VISA is required for its degradation mediated by RNF146. Interestingly, RNF146-mediated degradation of VISA could be inhibited by the proteasomal inhibitor MG132 but not the lysosomal inhibitor NH_4Cl or the autophagic inhibitor 3-methyladenine or chloroquine, suggesting that RNF146 mediates degradation of VISA via a proteasomal pathway (Fig. 6*I*). To further determine the role of RNF146 in the regulation of the stability of VISA, we generated RNF146-deficient (RNF146-KO) HEK293 cell pools by the CRISPR-Cas9 system. As shown in Fig. 6*J*, RNF146 deficiency delayed the degradation of VISA after SeV infection. These data suggest that RNF146 mediates proteasome-dependent degradation of VISA.

We further investigated whether RNF146 promoted polyubiquitination of VISA. As shown in Fig. 6*K*, overexpression of RNF146 markedly increased K48-linked but not K63-linked polyubiquitination of VISA, whereas RNF146 deficiency markedly impaired SeV-triggered K48- but not K63-linked polyubiquitination of VISA in comparison with control cells (Fig. 6*L*). To determine which lysine residues in VISA were targeted by RNF146 for K48-linked polyubiquitination, we carried out a systematic lysine (K) to arginine (R) mutation scanning and

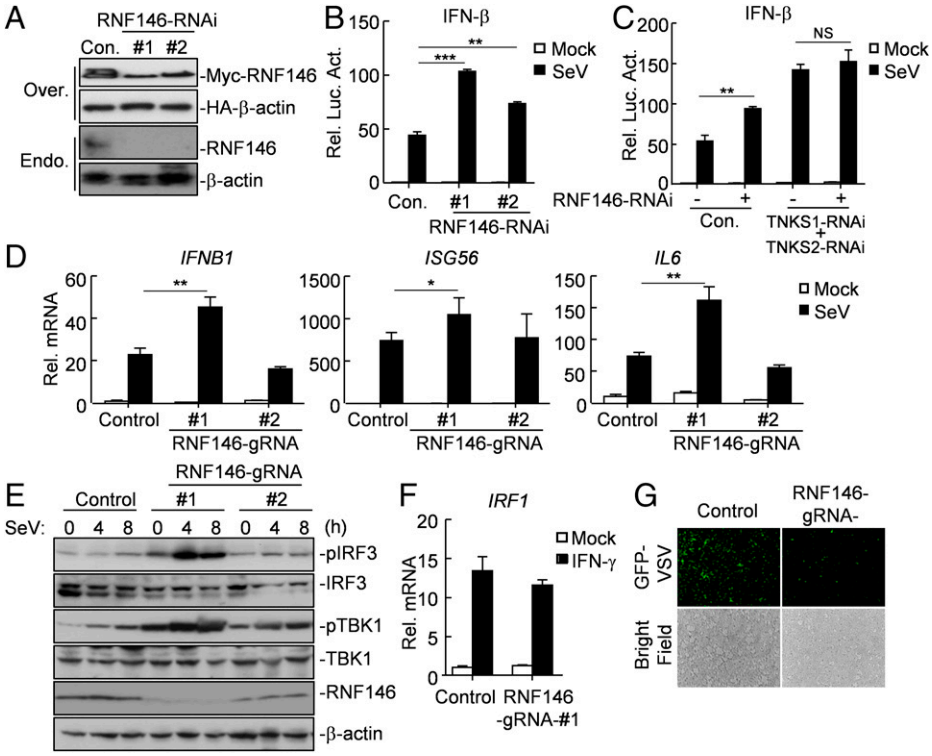

Fig. 7. RNF146 negatively regulates virus-triggered signaling. (*A*) Effects of RNF146-RNAi on the expression of RNF146. As shown in *Upper*, HEK293 cells (2×10^5) were transfected with Myc-RNF146 (0.1 μg), HA-β-actin (0.01 μg), and the indicated RNF146-RNAi plasmids (0.5 μg) for 36 h before immunoblotting analysis. As shown in *Lower*, HEK293 cells (2×10^5) were transfected with the indicated RNF146-RNAi plasmids (2 μg) for 12 h. The cells were then selected with puromycin (1 μg/mL) for 24 h before immunoblotting analysis. (*B*) Effects of RNF146-RNAi on SeV-triggered activation of the IFN-β promoter. HEK293 cells (1×10^5) were transfected with IFN-β promoter (0.1 μg) and pRL-TK *Renilla* luciferase reporter plasmid (0.01 μg) along with the indicated RNAi plasmids (0.5 μg) for 36 h, and the cells were then untreated or infected with SeV for 10 h before luciferase assays. (*C*) Effects of double knockdown of TNKS1 and TNKS2 on the synergistic activation of the IFN-β promoter induced by SeV and RNF146 knockdown. HEK293 cells (1×10^5) were transfected with IFN-β promoter (0.1 μg) and pRL-TK *Renilla* luciferase reporter plasmid (0.01 μg) along with the indicated RNAi plasmids (0.5 μg) for 36 h, and the cells were then untreated or infected with SeV for 10 h before luciferase assays. (*D*) Effects of RNF146 deficiency on the SeV-triggered transcription of downstream genes in HEK293 cells. RNF146-deficient (RNF146-KO) HEK293 cells were generated by the CRISPR-Cas9 system. Then, the RNF146-KO and control HEK293 cells (2×10^5) were untreated or infected with SeV for 10 h before qRT-PCR analysis. (*E*) Effects of RNF146 deficiency on the SeV-triggered phosphorylation of TBK1 and IRF3. The RNF146-KO and control HEK293 cells (4×10^5) were untreated or infected with SeV for the indicated time points before immunoblotting analysis. (*F*) Effects of RNF146 deficiency on the IFN-γ–triggered transcription of downstream genes. The RNF146-KO and control HEK293 cells (2×10^5) were untreated or treated with IFN-γ (50 ng/mL) for 4 h before qRT-PCR analysis. (*G*) Effects of RNF146 deficiency on the replication of GFP-VSV. The RNF146-KO and control HEK293 cells (2×10^5) were infected with GFP-VSV for 24 h and imaged by microscopy. Data are represented as the mean ± SEM. NS, no significance. **P* < 0.05 (Student's *t* test); ***P* < 0.01 (Student's *t* test); ****P* < 0.001 (Student's *t* test). Con., control; Rel. Luc. Act., relative luciferase activity.

tested the effects of RNF146 on their stabilities. As shown in *SI Appendix*, Fig. S7*A*, protein levels of all mutants except VISA (K7R) were markedly reduced by RNF146. Consistently, RNF146 mediated polyubiquitination of the wild type but not VISA(K7R) (*SI Appendix*, Fig. S7*B*). Collectively, these results suggest that RNF146 directly mediates K48-linked polyubiquitination of VISA at K7 and promotes its proteasomal degradation after virus infection.

RNF146 Negatively Regulates Virus-Triggered Signaling. As RNF146 mediated the polyubiquitination and degradation of VISA, we next determined the roles of RNF146 in the regulation of RNA virus–triggered innate immune signaling. Reporter assays indicated that overexpression of RNF146 inhibited SeV-triggered activation of the IFN-β promoter in a dose-dependent manner (*SI Appendix*, Fig. S8*A*). To further probe its roles in virus trigger signaling, we used two RNF146-RNAi plasmids (pGIPZ-RNF146-RNAi-#1 and -#2) from the laboratory of Chen and coworkers (36), which could inhibit the expression of transfected and endogenous RNF146 (Fig. 7*A*). In reporter assays, knockdown of RNF146 potentiated SeV-induced activation of the IFN-β promoter in control cells (Fig. 7*B*). but not in TNKS1 and TNKS2 double knockdown cells (Fig. 7*C*), suggesting that TNKS1 and TNKS2 are required for RNF146 to exert its function. By contrast, neither overexpression nor knockdown of RNF146 affected IFN-γ–triggered activation of the IRF1 promoter (*SI Appendix*, Fig. S8 *B* and *C*). To further determine the roles of endogenous RNF146, we generated RNF146-deficient HEK293 cell pools by using three independent RNF146 guide RNAs (gRNAs). RNF146-gRNA-#1 and RNF146-gRNA-#3 but not RNF146-gRNA-#2 dramatically inhibited the expression of RNF146 (Fig. 7*E* and *SI Appendix*, Fig. S8*D*). qRT-PCR analysis indicated that RNF146 deficiency (generated by using RNF146-gRNA-#1 or -#3) potentiated SeV-induced transcription of downstream antiviral genes, including *IFNB1*, *ISG56*, and *IL6*, compared with control cells (Fig. 7*D* and *SI Appendix*, Fig. S8*D*). In addition, phosphorylation of TBK1 and IRF3 induced by SeV was dramatically increased in RNF146-deficient HEK293 cells in comparison with control cells (Fig. 7*E*). By contrast, IFN-γ–induced transcription of *IRF1* was comparable between RNF146-deficient and control HEK293 cells (Fig. 7*F*). Consistently, RNF146 deficiency impaired the replication of GFP-VSV compared with the control cells (Fig. 7*G*). Collectively, these results suggest that RNF146 negatively regulates RNA virus–triggered innate immune signaling.

Discussion

VISA is an essential adaptor protein that mediates innate immune response to RNA viruses, and many proteins modulate innate immune response by impinging on this key regulatory node. Exploring the mechanisms of VISA activation and regulation can help us to understand how the innate immune system mounts an appropriate response to clear the infected virus but avoids overresponse that could cause harmful immune damage. In this study, we identified PARylation and subsequent degradation of VISA by the TNKS–RNF146 axis as a regulatory mechanism to attenuate the VISA-mediated innate immune response.

Posttranslation modification of VISA is an important way to regulate VISA-mediated antiviral response; here, we find PARylation as a form of PTM of VISA. Several lines of evidences indicated that VISA/MAVS is a substrate of TNKS1/2, and the PARylation of VISA/MAVS by TNKS1/2 can serve as a signal for RNF146-mediated polyubiquitination and degradation. We first identified TNKS1 and TNKS2 as VISA-associated proteins and found that they interacted with the TNKS-binding motif of VISA through their ANK region, which is responsible for binding their substrates. Subsequently, we found that viral infection led to the induction of TNKS1 and TNKS2, which translocated from cytosol to mitochondria to interact with VISA. Consistently, endogenous TNKS1 and TNKS2 were weakly associated with VISA in uninfected cells, and their association was increased after SeV infection. These results indicate that VISA is a substrate for TNKS. In agreement with this, overexpression of TNKS1 or TNKS2 but not their catalytically inactive mutants increased PARylation of VISA at E137, whereas deficiency of either TNKS1 or TNKS2 impaired the virus-triggered PARylation of VISA. Thus, both TNKS1 and TNKS2 mediated PARylation of VISA following virus infection. Recent studies suggested that the E3 ligase RNF146 recognized TNKS substrates and promoted their proteasome-dependent degradation (39). Consistent with this, we showed that RNF146 associated with PARylated VISA through its WWE domain, which is responsible for the recognition of the ADP ribosylated proteins, and promoted VISA degradation. Furthermore, TNKS inhibitors could inhibit the interaction between RNF146 and VISA. In addition, simultaneous knockdown of both TNKS1 and TNKS2 inhibited the synergistically activation of the IFN-β promoter induced by SeV and RNF146 knockdown. VISA-AA, which is impaired in interaction with TNKS1 or TNKS2, also lost its ability to interact with RNF146 and be degraded by overexpression of RNF146. In addition, RNF146 also cannot mediate degradation of VISA-E137A, the mutant that could not be PARylated by TNKS. These results suggest that PARylated VISA was recognized by RNF146. Interestingly, RNF146 promoted K48- but not K63-linked polyubiquitination of VISA at K7 after SeV infection, which is important for its degradation in a proteasome-dependent manner. Overall, these results suggest that the TNKS–RNF146 axis mediates the PARylation, polyubiquitination, and consequently, degradation of VISA (*SI Appendix*, Fig. S9).

Our results demonstrate that PARylation and subsequent degradation of VISA by the TNKS–RNF146 axis specifically inhibited virus-triggered expression of type I IFNs and the innate antiviral response. Overexpression of TNKS1, TNKS2, or RNF146 inhibited the virus-triggered activation of IFN-β, while knockdown or knockout of TNKS1, TNKS2, or RNF146 had the opposite effect. TNKS1 or TNKS2 deficiency potentiated SeV-, EMCV-, or cytoplasmic-transfected dsRNA-triggered induction of downstream effector genes in different types of cells. Moreover, the replication of GFP-tagged VSV was decreased in RNF146-, TNKS1- or TNKS2-deficient cells compared with that in control cells. In vivo experiments indicated that the serum cytokines, such as IFN-β, IL-6, and MCP1, induced by infection with EMCV or PR8 were significantly increased in TNKS1- or TNKS2-deficient mice in comparison with their control littermates. Consistently, the transcription of *Ifnb1* and *Isg56* was increased, while the EMCV genomic copy numbers were impaired in the brains and lungs from TNKS1- or TNKS2-deficient mice compared with their wild-type counterparts after virus infection. These results demonstrate that PARylation of VISA by TNKS1 and TNKS2 attenuates innate immune response to RNA viruses in vivo. Unfortunately, we were unable to investigate the role of RNF146 in vivo because RNF146-deficient mice exhibit early embryonic lethality due to delayed bone formation in the calvarium (44).

TNKS1 and TNKS2 have been implicated in many cellular processes, including telomere homeostasis, glucose metabolism, and so on. Here, we found that they have a functional overlap in innate antiviral response, which reflects the potential nonredundant roles of TNKS1 and TNKS2. Both TNKS1 and TNKS2 can PARylate VISA to down-regulate innate antiviral response. Consistently, knockdown or knockout of TNKS1 or TNKS2 potentiated virus-triggered innate immune response, while simultaneous knockdown or knockout of both TNKS1 and TNKS2 markedly enhanced the SeV-induced activation of the IFN-β compared with knockdown of each individually. Unfortunately, *Tnks1* and *Tnks2* double-knockout mice are embryonically lethal (45), which hurdled our investigation of their roles in double-knockout mice.

Interestingly, although TNKS1-deficient mice and TNKS2-deficient mice produced a similar cytokine profiles postviral infection, we observed that TNKS2-deficient mice were more resistant to virus infection as expected, whereas TNKS1-deficient mice were more susceptive to EMCV- or PR8-induced death. This unexpected phenotype of TNKS1-deficient mice suggests that TNKS1 and TNKS2 may function differently in the pathological changes of different organs or tissues postvirus infection, although they have comparable effects on antiviral innate immune response. Consistent with this, qRT-PCR analysis indicated that *Tnks1* but not *Tnks2* was expressed in the liver of mice. Moreover, we observed that the livers from TNKS1- but not TNKS2-deficient mice were much smaller and exhibited serve damage after virus infection. These results suggest that TNKS1 and TNKS2 function in a tissue-specific manner. Interestingly, it has been reported that deficiency of TNKS1 in mice enhances energy expenditure, insulin sensitivity, and fatty acid oxidation and exhibits reduced adiposity (38). These findings suggest that deficiency of TNKS1 results in liver metabolic disorders. TNKS1-deficient mice exhibited more severe liver damage and are susceptive to EMCV and PR8 infection; this may be due to their metabolic disorders postvirus infection, which will be characterized in a separate study.

In conclusion, our study suggests that PARylation of VISA by TNKS1/2 can serve as a signal for RNF146-mediated polyubiquitination and degradation after virus infection, which represents a regulatory mechanism for the feedback regulation of VISA-mediated innate antiviral response (*SI Appendix*, Fig. S9). Recently, the expression of TNKS1 and TNKS2 was shown to be up-regulated after severe acute respiratory syndrome coronavirus 2 (SARS-CoV-2) infection by RNA-sequencing analysis (46), which is consistent with our finding that TNKS1 and TNKS2 are up-regulated after RNA virus infection and negatively regulate innate immune response to RNA viruses. TNKS inhibitor has also been reported to enhance the antitumor effect of anti–PD-L1 antibody by up-regulating the inflammatory proteins (e.g., CCL3 and CCL4), which attracted $CD8^+$ T cells in the tumor microenvironment (43). These reports in combination with our findings suggest that targeting TNKS by its inhibitors to enhance innate immune and inflammatory response might be a strategy to treat RNA virus infections and tumors.

Materials and Methods

All animal experiments were performed in accordance with the Wuhan University Animal Care and Use Committee guidelines. Information on reagents, antibodies, cells, constructs, PCR primers, and RNAi target sequences is described in *SI Appendix, SI Materials and Methods*. The methods for generation of bone marrow–derived monocytes and BMDMs, isolation of MLFs, cell lines, retroviral gene transfer, transfection, reporter assays, Co-IP, immunoblot analysis, and statistical analysis are previously described (47), and the details are presented in *SI Appendix, SI Materials and Methods*.

Data Availability. All study data are included in the article and/or *SI Appendix*.

ACKNOWLEDGMENTS. We thank Dr. Richard J. Hodes (NIH) and Dr. Yeguang Chen (Tsinghua University, China) for providing the TNKS1- and TNKS2-deficient mice and Dr. Hongbing Shu (Wuhan University, China) and Dr. Junjie Chen (MD Anderson Cancer Center) for providing a series of key reagents. This work was supported by National Natural Science Foundation of China Grants 32070773, 31870870, and 31871411; Fundamental Research Funds for the Central Universities Grant 2042022kf1192; State Key Laboratory of Veterinary Etiological Biology Grant SKLVEB2020KFKT002; the Young Top-Notch Talent Cultivation Program of Hubei Province; and Wuhan University Experiment Technology Project Funding Grant WHU-2020-SYJS-05.

Author affiliations: [a]State Key Laboratory of Virology, College of Life Sciences, Wuhan University, Wuhan 430072, China; [b]Hubei Key Laboratory of Cell Homeostasis, College of Life Sciences, Wuhan University, Wuhan 430072, China; [c]Frontier Science Center for Immunology and Metabolism, Wuhan University, Wuhan 430071, China; [d]Tongji School of Pharmacy, Huazhong University of Science & Technology, Wuhan 430030, China; and [e]State Key Laboratory of Veterinary Etiological Biology, Lanzhou Veterinary Research Institute, Chinese Academy of Agricultural Sciences, Lanzhou 730000, China

1. S. Akira, S. Uematsu, O. Takeuchi, Pathogen recognition and innate immunity. *Cell* **124**, 783–801 (2006).
2. R. B. Seth, L. Sun, C. K. Ea, Z. J. Chen, Identification and characterization of MAVS, a mitochondrial antiviral signaling protein that activates NF-kappaB and IRF 3. *Cell* **122**, 669–682 (2005).
3. L. G. Xu *et al.*, VISA is an adapter protein required for virus-triggered IFN-beta signaling. *Mol. Cell* **19**, 727–740 (2005).
4. T. Kawai *et al.*, IPS-1, an adaptor triggering RIG-I- and Mda5-mediated type I interferon induction. *Nat. Immunol.* **6**, 981–988 (2005).
5. E. Meylan *et al.*, Cardif is an adaptor protein in the RIG-I antiviral pathway and is targeted by hepatitis C virus. *Nature* **437**, 1167–1172 (2005).
6. S. Liu *et al.*, MAVS recruits multiple ubiquitin E3 ligases to activate antiviral signaling cascades. *eLife* **2**, e00785 (2013).
7. F. Hou *et al.*, MAVS forms functional prion-like aggregates to activate and propagate antiviral innate immune response. *Cell* **146**, 448–461 (2011).
8. S. M. Belgnaoui, S. Paz, J. Hiscott, Orchestrating the interferon antiviral response through the mitochondrial antiviral signaling (MAVS) adapter. *Curr. Opin. Immunol.* **23**, 564–572 (2011).
9. B. Liu *et al.*, The ubiquitin E3 ligase TRIM31 promotes aggregation and activation of the signaling adaptor MAVS through Lys63-linked polyubiquitination. *Nat. Immunol.* **18**, 214–224 (2017).
10. X. He *et al.*, RNF34 functions in immunity and selective mitophagy by targeting MAVS for autophagic degradation. *EMBO J.* **38**, e100978 (2019).
11. K. Arimoto *et al.*, Negative regulation of the RIG-I signaling by the ubiquitin ligase RNF125. *Proc. Natl. Acad. Sci. U.S.A.* **104**, 7500–7505 (2007).
12. C. Castanier *et al.*, MAVS ubiquitination by the E3 ligase TRIM25 and degradation by the proteasome is involved in type I interferon production after activation of the antiviral RIG-I-like receptors. *BMC Biol.* **10**, 44 (2012).
13. B. Zhong *et al.*, The E3 ubiquitin ligase RNF5 targets virus-induced signaling adaptor for ubiquitination and degradation. *J. Immunol.* **184**, 6249–6255 (2010).
14. Y. S. Yoo *et al.*, The mitochondrial ubiquitin ligase MARCH5 resolves MAVS aggregates during antiviral signalling. *Nat. Commun.* **6**, 7910 (2015).
15. X. Zhou, F. You, H. Chen, Z. Jiang, Poly(C)-binding protein 1 (PCBP1) mediates housekeeping degradation of mitochondrial antiviral signaling (MAVS). *Cell Res.* **22**, 717–727 (2012).
16. F. You *et al.*, PCBP2 mediates degradation of the adaptor MAVS via the HECT ubiquitin ligase AIP4. *Nat. Immunol.* **10**, 1300–1308 (2009).
17. Y. Pan *et al.*, Smurf2 negatively modulates RIG-I-dependent antiviral response by targeting VISA/MAVS for ubiquitination and degradation. *J. Immunol.* **192**, 4758–4764 (2014).
18. Y. Wang, X. Tong, X. Ye, Ndfip1 negatively regulates RIG-I-dependent immune signaling by enhancing E3 ligase Smurf1-mediated MAVS degradation. *J. Immunol.* **189**, 5304–5313 (2012).
19. T. Liuyu *et al.*, Induction of OTUD4 by viral infection promotes antiviral responses through deubiquitinating and stabilizing MAVS. *Cell Res.* **29**, 67–79 (2019).
20. S. Liu *et al.*, Phosphorylation of innate immune adaptor proteins MAVS, STING, and TRIF induces IRF3 activation. *Science* **347**, aaa2630 (2015).
21. W. Xiang *et al.*, PPM1A silences cytosolic RNA sensing and antiviral defense through direct dephosphorylation of MAVS and TBK1. *Sci. Adv.* **2**, e1501889 (2016).
22. B. R. Yan *et al.*, PKACs attenuate innate antiviral response by phosphorylating VISA and priming it for MARCH5-mediated degradation. *PLoS Pathog.* **13**, e1006648 (2017).
23. T. Li *et al.*, O-GlcNAc transferase links glucose metabolism to MAVS-mediated antiviral innate immunity. *Cell Host Microbe* **24**, 791–803.e6 (2018).
24. J. Zhu *et al.*, Arginine monomethylation by PRMT7 controls MAVS-mediated antiviral innate immunity. *Mol. Cell* **81**, 3171–3186.e8 (2021).
25. R. Gupte, Z. Liu, W. L. Kraus, PARPs and ADP-ribosylation: Recent advances linking molecular functions to biological outcomes. *Genes Dev.* **31**, 101–126 (2017).
26. T. Yamada *et al.*, Constitutive aryl hydrocarbon receptor signaling constrains type I interferon-mediated antiviral innate defense. *Nat. Immunol.* **17**, 687–694 (2016).
27. T. Guo *et al.*, ADP-ribosyltransferase PARP11 modulates the interferon antiviral response by mono-ADP-ribosylating the ubiquitin E3 ligase β-TrCP. *Nat. Microbiol.* **4**, 1872–1884 (2019).
28. P. Verheugd *et al.*, Regulation of NF-κB signalling by the mono-ADP-ribosyltransferase ARTD10. *Nat. Commun.* **4**, 1683 (2013).
29. G. Gao, X. Guo, S. P. Goff, Inhibition of retroviral RNA production by ZAP, a CCCH-type zinc finger protein. *Science* **297**, 1703–1706 (2002).
30. X. Guo, J. Ma, J. Sun, G. Gao, The zinc-finger antiviral protein recruits the RNA processing exosome to degrade the target mRNA. *Proc. Natl. Acad. Sci. U.S.A.* **104**, 151–156 (2007).
31. Y. Zhang *et al.*, PARP9-DTX3L ubiquitin ligase targets host histone H2BJ and viral 3C protease to enhance interferon signaling and control viral infection. *Nat. Immunol.* **16**, 1215–1227 (2015).
32. S. J. Hsiao, S. Smith, Tankyrase function at telomeres, spindle poles, and beyond. *Biochimie* **90**, 83–92 (2008).
33. S. Guettler *et al.*, Structural basis and sequence rules for substrate recognition by Tankyrase explain the basis for cherubism disease. *Cell* **147**, 1340–1354 (2011).
34. W. Chang, J. N. Dynek, S. Smith, TRF1 is degraded by ubiquitin-mediated proteolysis after release from telomeres. *Genes Dev.* **17**, 1328–1333 (2003).
35. S. M. Huang *et al.*, Tankyrase inhibition stabilizes axin and antagonizes Wnt signalling. *Nature* **461**, 614–620 (2009).
36. N. Li *et al.*, Poly-ADP ribosylation of PTEN by tankyrases promotes PTEN degradation and tumor growth. *Genes Dev.* **29**, 157–170 (2015).
37. B. Liu, C. Gao, Regulation of MAVS activation through post-translational modifications. *Curr. Opin. Immunol.* **50**, 75–81 (2018).
38. T. Y. Yeh *et al.*, Hypermetabolism, hyperphagia, and reduced adiposity in tankyrase-deficient mice. *Diabetes* **58**, 2476–2485 (2009).
39. Y. Zhang *et al.*, RNF146 is a poly(ADP-ribose)-directed E3 ligase that regulates axin degradation and Wnt signalling. *Nat. Cell Biol.* **13**, 623–629 (2011).
40. C. M. Daniels, S. E. Ong, A. K. Leung, The promise of proteomics for the study of ADP-ribosylation. *Mol. Cell* **58**, 911–924 (2015).
41. Y. Zhang, J. Wang, M. Ding, Y. Yu, Site-specific characterization of the Asp- and Glu-ADP-ribosylated proteome. *Nat. Methods* **10**, 981–984 (2013).
42. N. Levaot *et al.*, Loss of Tankyrase-mediated destruction of 3BP2 is the underlying pathogenic mechanism of cherubism. *Cell* **147**, 1324–1339 (2011).
43. P. A. DaRosa *et al.*, Allosteric activation of the RNF146 ubiquitin ligase by a poly(ADP-ribosyl)ation signal. *Nature* **517**, 223–226 (2015).
44. Y. Matsumoto *et al.*, Ubiquitin ligase RNF146 coordinates bone dynamics and energy metabolism. *J. Clin. Invest.* **127**, 2612–2625 (2017).
45. Y. J. Chiang *et al.*, Tankyrase 1 and tankyrase 2 are essential but redundant for mouse embryonic development. *PLoS One* **3**, e2639 (2008).
46. C. D. Heer *et al.*, Coronavirus infection and PARP expression dysregulate the NAD metabolome: An actionable component of innate immunity. *J. Biol. Chem.* **295**, 17986–17996 (2020).
47. C. Q. Lei *et al.*, USP19 inhibits TNF-α- and IL-1β-triggered NF-κB activation by deubiquitinating TAK1. *J. Immunol.* **203**, 259–268 (2019).